

A method for prevent water inrush from karst collapse column: a case study from Sima mine, China

Hao Li¹ · Haibo Bai¹ · Jianjun Wu² · Huiming Zhao¹ · Kai Ma¹

Received: 23 February 2017 / Accepted: 14 July 2017 / Published online: 19 July 2017
© Springer-Verlag GmbH Germany 2017

Abstract Mining-induced groundwater inrush could result in serious economic losses and casualties. This disaster usually depends on geological structure, such as the karst collapse column (KCC). It could reduce the aquifuge thickness, causing a great risk of water bursting. In order to assess the impact of mining on the KCC, we have developed a complete set of methods, including three-dimensional seismic exploration, connectivity experiment, water injection experiment in two sidewalls, numerical simulation based on Drucker–Prager (D–P) elastoplastic damage theory. This method is used to test the size, type and the damage thickness of the KCC named DX1 in Sima mine, and the results indicate that the type of DX1 is good cementation. In addition, under the influence of the shear stress at the coal wall and the unloading at the goaf, a significant compressive damage zone with a large damage thickness will form at the sidewall of the KCC. As the roof collapses, the backfill is compacted and the maximum damage thickness gradually moves to the other side of the KCC. Eventually, an asymmetric inverted saddle-shaped damage distribution is formed with a maximum compression damage depth of 32.5 m. The results provide a basis for preventing water inrush from KCC.

Keywords Karst collapse column · Connectivity experiment · Water injection experiment · Elastoplastic damage model · Numerical simulation

Introduction

More than 90% of China's coal output is produced in North China, and about 300 billion tons of proven reserves are threatened by Ordovician karst aquifers. In the past 60 years, more than 1300 groundwater inrush accidents occurred, which resulted in heavy casualties and economic losses due to the thin water barrier and complicated geological structure (Huang et al. 2014; Wang et al. 2012; Wu et al. 2013).

In Carboniferous Permian coalfields in north China, especially in Shanxi Province, there is a concealed vertical geological phenomenon known as the karst collapse column (KCC), which is caused by the karst subsidence that occurs in Ordovician limestone aquifer (Li and Zhou 2006). The cave gradually expands, collapses and penetrates the coal seam, eventually forming a plug-shaped geological structure (Fig. 1). According to the cementing degree of filling in the column, the KCC can be divided into two types: good cementation type (no water in column) and poor cementation type, including column filled with water and the edge of column filled with water. However, no matter what type the KCC is, it could lead to the loss of coal reserves (Hao et al. 2015). More importantly, this weak geological structure may be the water channel between the Ordovician limestone aquifer and the working face under the mining influence (He et al. 2007).

Between 1950s and 1990s, people mainly study the causes, shape, distribution and detecting method of KCC (Qian 1988; Yuan 1994; Shi et al. 1998). With the increase in the coal mining depth, the serious water groundwater inrush caused by the activation of KCC happened in many mines (Zhou and Yang 1999; Yin et al. 2005; Zhang et al. 2009); thus, many scholars have used different methods to prevent these disasters in recent years. Yin and Zhang

✉ Haibo Bai
hbbaicumtedu@126.com

¹ State Key Laboratory for Geomechanics and Deep Underground Engineering, China University of Mining and Technology, Xuzhou 221116, Jiangsu, China

² Shanxi China Coal Huajin Energy Limited Liability Company, Hejin 043300, Shanxi, China

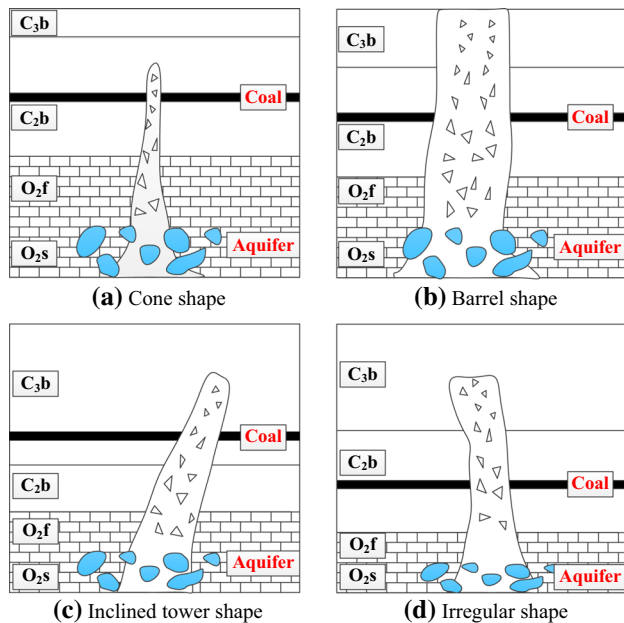


Fig. 1 Four profile shapes of KCC

(2005) studied displacement of KCC under the mining influence by numerical simulation method. Zhu and Wei (2011) used the “strain method” to test the strain of floor rock mass during mining advance, monitoring the deformation of rock strata in different depths. Ou et al. (2013) analyzed the distribution of the plastic zone in the poor-cementation-type KCC by numerical simulation. Li et al. (2016) and Zhang and Tu (2016) obtained the stress analytic solution of surrounding rock based on the hypothesis that rock mass was linear elastic material and the cross section of the collapse column was circular. Using the elastic–plastic theory and single sidewall water injection test, Ma et al. (2016) concluded that the failure depth of poor-cementation-type KCC reaches the maximum when the mining face advances to the KCC.

The methods of analytic, numerical simulation, strain test or single sidewall water injection test were used in the above literature. However, only one method cannot predict the water inrush risk of KCC accurately. For the in-site test, the above strain test and single sidewall water injection test cannot judge the location of the maximum damage thickness of the KCC. Under the mining influence, the KCC bears cyclic loading of compression–tension–compression as well as the continuous confined water pressure. The rock in the column is damaged in this stress path. For the numerical and analytical methods, it is difficult to reasonably reflect this stress path by using the traditional constitutive model. More importantly, they did not employ a simple and appropriate method to distinguish the KCC’s type, which had a significant impact on the water-transmitting ability of KCC. A new method that is more

consistent with the damage law of the KCC has been developed, as shown in Fig. 2. The shape and size of the KCC are obtained by three-dimensional (3D) seismic exploration. On these bases, a “connectivity experiment” was used to determine the type of KCC. Instead of “strain method” and “single sidewall water injection test,” this article used the “water injection experiment in two side-walls” to test the damage thickness at some points in the KCC’s sidewall where there is a high probability of water inrush. The damage law can be obtained by combining the results of numerical simulation based on D–P elastoplastic damage theory. By these methods, we find that the position of maximum damage thickness of the KCC is not at the sidewall near the starting cut (Yin et al. 2005; Ma et al. 2016), which most scholars believed, but at the sidewall away from the starting cut. This conclusion provides a basis for coal mine safety production.

Study area

Overview of the Sima Mine

The Sima mine is located in the north of Jincheng, Shanxi Province. It lies in the south of Qinshui coalfield, covers an area of 30.7 km² (Fig. 3) and has an annual coal production of 2.2 million tons. The primary mineable coal seam is no. 15 with a 4 m thickness.

The most significant geological structure in Sima mine is KCC. As shown in Fig. 3. Thirty-six KCCs mainly distribute in the northwest of the coal mine. The existence of the KCCs will not only affect the layout of the working face, but also may be the underground watercourse between Ordovician limestone aquifer and the stopes. Especially for the KCC named DX1 in 3152 working face, it is located in the karst development area; therefore, it has a high risk of water inrush from the geological aspects. In other words, as long as it has been proved that DX1 is safe, the rest KCCs of Sima mine are theoretically safe. Based

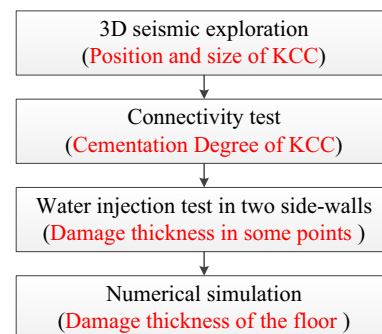


Fig. 2 The set of methods to prevent water inrush from KCC

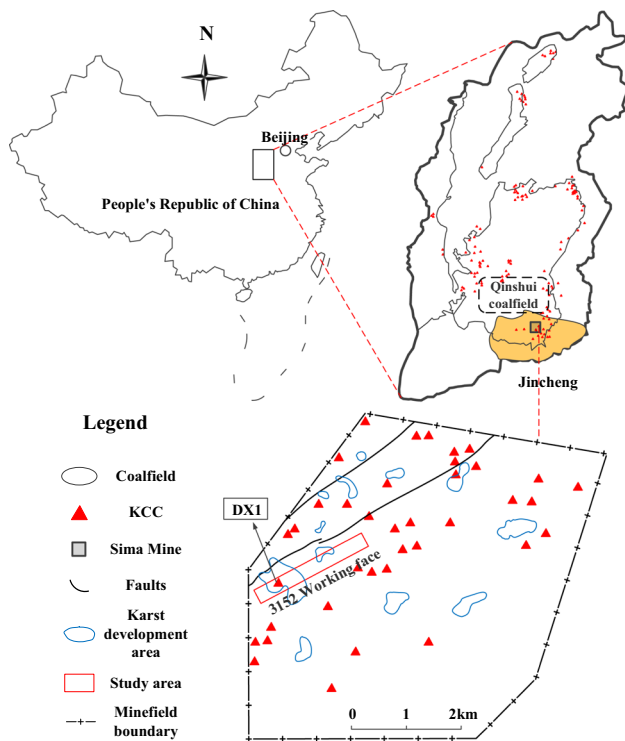


Fig. 3 Location of the Sima mine

on the above analysis, DX1 and 3152 working face were selected as the study area (red box in Fig. 3).

Engineering situation

As shown in Fig. 4, the working face 3152 has an overburden depth of 620 m and is 2070 m in the dip direction and 230 m in the strike direction. Longwall mining is employed with backward extraction. The distance from DX1 to the starting cut is about 800 m, and the distance from DX1 to 3152 coal haulage roadway is 62 m. According to the 3D seismic data, the DX1 is the cone shape; its diameter is 11.5 m in the 3152 working face. According to the drilling data, a part of 3152 working face is located in the middle karst development area with the confined water pressure of 2 MPa. Ordovician Fengfeng Formation (O₂f) and Carboniferous Benxi Formation (C₂b) are aquifuges in which the minimum thickness is 57 m. The aquifuge is thick enough to ensure the safety of the complete floor. However, the existence of DX1 destroyed the integrity of the floor, and its weak mechanical properties make the aquifuge thickness greatly reduce under the mining influence, causing a greater risk of water bursting.

According to the methods shown in Fig. 1, the position and size of DX1 are determined by the three-dimensional seismic data. On this basis, we developed a “connectivity test” method to determine the KCC’s type.

In situ test

Connectivity test

Connectivity test is an effective method to determine the type of KCC. By injecting high-pressure water continuously into one hole and observing the water flow of the other one, the rupture of rock mass between the two holes can be determined. The experiment was carried out by drilling three oblique drilling holes T₀₁, T₀₂ and T₀₃ into the middle of the KCC with the vertical depths of 26, 30 and 34 m respectively (Figs. 4, 5). The T₀₂ was treated as the observation hole, and T₀₁ and T₀₃ were treated as water injection hole in two experiments. The water pressure in T₀₁ or T₀₃ gradually increased from 0 until the water burst phenomenon occurred in T₀₂. The experimental results of water flow at different water pressure conditions are shown in Tables 1 and 2.

Tables 1 and 2 show that DX1 has a good water-blocking capacity. The water flow in T₀₁ and T₀₃ increases with the increase in water injection pressure, but observation hole T₀₂ had no water leakage phenomenon when water injection pressure in T₀₁ and T₀₃ was less than 5 Ma. Once the water pressure exceeded 5 MPa, T₀₂ hole began to seep, a large amount of water inrush occurred as time went on and water pressure increased. The water inflow of the T₀₃ hole began to increase greatly when the water pressure reached 5.5 MPa, which indicated that the cracks gradually developed and penetrated under the action of water pressure splitting, resulting in a dramatic increase in the amount of water. Compared the two groups of connectivity test, the water inflow in T₀₁ hole was more than the T₀₃, and the water pressure in T₀₁ hole is less than T₀₃.

The above results indicate that the permeability between the T₀₃ and T₀₂ is worse than that between the T₀₁ and T₀₂. In other words, the water isolating capacity of DX1 will increase with the increase of burial depth. Therefore, DX1 belongs to the good cementation type and has no risk of water inrush if the water pressure is less than 2 MPa. A plugging operation is required after this experiment to avoid interfering with the results of the “water injection test.”

Water injection test in two sidewalls

The shear stress in the floor could lead to the dislocation of the KCC and the surrounding rock during the mining advance, which leads to a shear sidewall channel for groundwater inrush (Ma et al. 2016). In order to evaluate the damage effect of shear stress at different sidewalls, we designed two sets of water injection experiments in the DX1: near the starting cut and away from the starting cut.

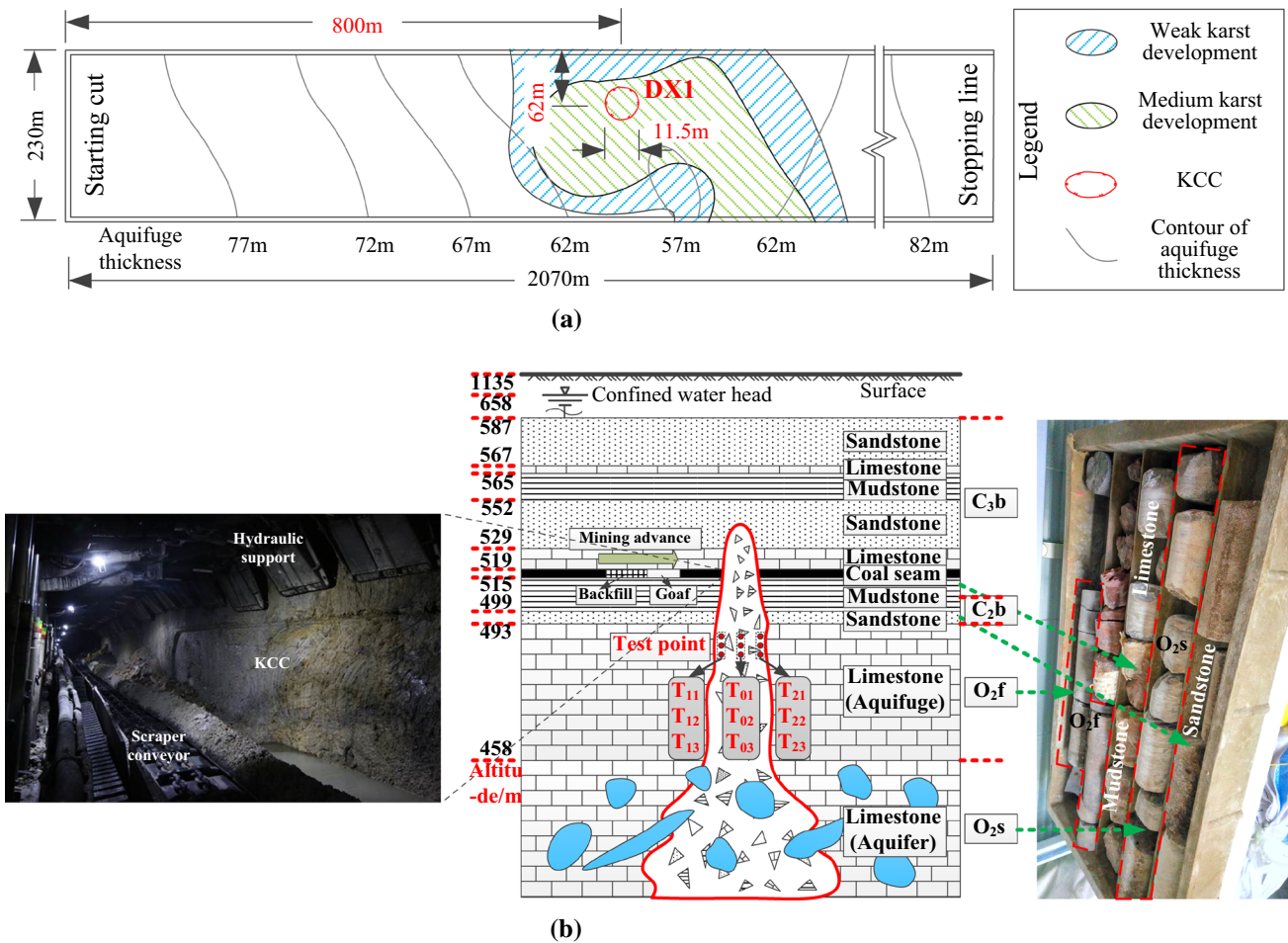


Fig. 4 Engineering situation of 3152 working face and the DX1. a DX1 plane position. b DX1 longitudinal profile

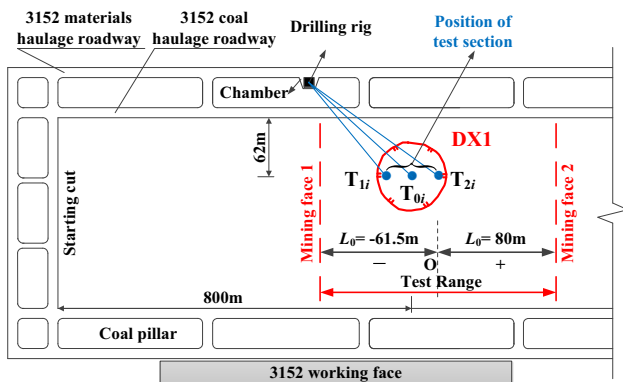


Fig. 5 The location of the test section

Unlike the connectivity experiment, in this test the water injection hole and the observation hole are the same. The test process is as follows: The drilling rig was placed in the 3152 materials haulage roadway, 800 m away from the starting cut (Fig. 5). We drilled oblique drillings in both the sidewalls of DX1, retained the 20-cm water injection section (T_{1i} and T_{2i} in Fig. 4, $i = 1, 2, 3$,

represents different depths) at the end of each borehole and set the steel pipe on the remaining length to prevent water loss. The vertical depths of these drilling were 26, 30 and 34 m, respectively. The water flow values of the holes were recorded if the distance between the working face and the T_{1i} was 50 m and no longer recorded if the distance between the working face and the T_{2i} was over 80 m. This experiment lasted a month and recorded the data shown in Fig. 6.

The results (Fig. 6) indicate that when the distance between the working face and the T_{1i} (left side of DX1) was more than 10 m, the water flow values of the three holes were almost zero, and the underground pressure did not cause damage to the DX1. When the working face was between T_{1i} and T_{2i} , the flow rate in T_{11} and T_{12} increased from 0 to 3.01 L/h and 1.60 L/h, respectively. The data indicate that the floor damage degree and range continued to increase due to mining effects. However, for T_{13} drilling, the water flow was kept at 0 L/h, which meant that the maximum damage thickness did not exceed 34 m. Water flow rate of T_{11} and T_{12} achieved a stable value,

Table 1 T_{01} and T_{02} connectivity experiment

Observation hole	Water pressure in T_{01} /Mpa	Injection time/min	Water flow/ m^3	Test result
T_{02}	0–2	15	0.058	No water in T_{02}
	2–4	15	0.105	No water in T_{02}
	4–5	15	0.287	No water in T_{02}
	5–5.5	15	0.538	Water burst from T_{02}

Table 2 T_{03} and T_{02} connectivity experiment

Observation hole	Water pressure in T_{03} /Mpa	Injection time/min	Water flow/ m^3	Test result
T_{02}	0–2	15	0.045	No water in T_{02}
	2–4	15	0.098	No water in T_{02}
	4–5	15	0.176	No water in T_{02}
	5–5.5	15	0.258	No water in T_{02}
	5.5–6	15	0.541	Water burst from T_{02}

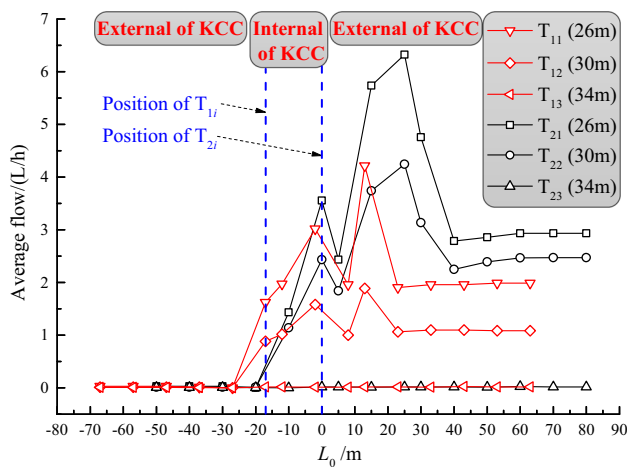


Fig. 6 Water injection test results in different depth

respectively, 1.99 and 1.08 L/h, until the working face passed T_{1i} as 50 m. In addition, the comparison of borehole T_{2i} and T_{1i} test data showed that the flow rates of the two have similar laws. Figure 6 shows that the water flow in the T_{2i} is significantly greater than that of T_{1i} . The test result indicates that the damage thickness on the left wall is less than that on the right wall, in which water inrush is more likely to occur.

Numerical simulation

Through the water injection test, it is possible to accurately obtain the damage thickness at some points during the mining process. However, numerical simulation is needed to obtain the damage thickness at each point of the floor, especially a reasonable interpretation of the results of the in situ test.

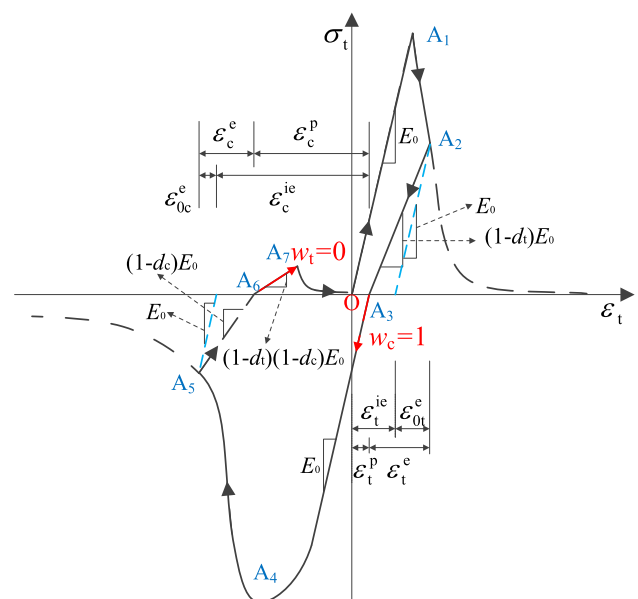


Fig. 7 Changes in mechanical properties during cyclic loading and unloading

Equations of D–P elastoplastic damage model

Compared to conventional constitutive models (Ou et al. 2013; Li et al. 2016), the D–P elastoplastic damage model can well reflect the changes in mechanical properties of rock materials during cyclic loading and unloading (Fig. 7), such as coal mining. Based on the Drucker–Prager yield criterion (Eq. 1), using the non-associated flow rule (Eq. 2), the plastic strain ϵ^p can be obtained.

In the effective stress space, the expression described by the hydrostatic stress \bar{p} and the deviatoric stress \bar{q} is (Lubliner et al. 1989; Lee and Fenves 1998)

$$F = [\bar{q} - 3\alpha\bar{p} + \beta\langle\bar{\sigma}_{imax}\rangle - \gamma\langle-\bar{\sigma}_{imax}\rangle]/(1 - \alpha) - \sigma_c = 0 \tag{1}$$

where $\alpha = [(\sigma_{b0}/\sigma_{c0}) - 1]/[2(\sigma_{b0}/\sigma_{c0}) - 1]$, $\beta = \bar{\sigma}_c/\bar{\sigma}_t$ ($1 - \alpha) - (1 + \alpha)$, $\gamma = 3(1 - K_c)/(2K_c - 1)$, $\bar{\sigma}_{imax}$ ($i = 1, 2, 3$) is the maximum principal effective stress; σ_{b0}/σ_{c0} is the ratio of initial equibiaxial compressive yield stress to initial uniaxial compressive yield stress; K_c is the ratio of the second stress invariant on the tensile meridian to that on the compressive meridian; and $\bar{\sigma}_c$ and $\bar{\sigma}_t$ are the effective tensile stress and the effective compressive stress, respectively.

The plastic potential function described by \bar{p} and \bar{q} is

$$G = \sqrt{(\delta\sigma_{t0} \tan \psi)^2 + \bar{q}^2} - \bar{p} \tan \psi \tag{2}$$

where δ is eccentricity that defines the rate at which the function approaches the asymptote; σ_{t0} is the uniaxial tensile stress at failure; and ψ is the dilation angle measured in the p - q plane at high confining pressure.

The relationship between stress and strain during cyclic loading and unloading is shown in Eq. 3.

$$\sigma = (1 - d)D_0^e(\varepsilon - \varepsilon^p) \tag{3}$$

where σ is the stress vector; D_0^e is the undamaged elastic stiffness matrix; ε is the total strain vector; ε^p is the plastic strain vector; d is determined by the stress state and the uniaxial damage variables, d_t and d_c , $1 - d = (1 - s_t d_c)(1 - s_c d_t)$; s_t and s_c are the function of stress, and $s_t = 1 - \omega_t r(\sigma_i)$, $s_c = 1 - \omega_c [1 - r(\sigma_i)]$, $0 \leq \omega_t, \omega_c \leq 1$, $i = 1, 2, 3$; σ_i ($i = 1, 2, 3$) are the principal stress components,

$$r(\sigma_i) = \sum_{i=1}^3 \langle\sigma_i\rangle / \sum_{i=1}^3 |\sigma_i|, \langle\sigma_i\rangle = (|\sigma_i| + \sigma_i)/2;$$

and ω_t and ω_c are weight factors, the values are shown in Fig. 7.

According to the geometric relationship shown in Fig. 7, the relationship between ε_t^p and d_t , ε_c^p and d_c can be deduced, as shown in Eqs. 4a and 4b, respectively.

$$\varepsilon_t^p = \varepsilon_t^{ie} - d_t \sigma_t / [(1 - d_t)E_0] \tag{4a}$$

$$\varepsilon_c^p = \varepsilon_c^{ie} - d_c \sigma_c / [(1 - d_c)E_0] \tag{4b}$$

where $\varepsilon_t^{ie} = \varepsilon_t - \varepsilon_{0t}^e = \varepsilon_t - \sigma_t/E_0$, $\varepsilon_c^{ie} = \varepsilon_c - \varepsilon_{0c}^e = \varepsilon_c - \sigma_c/E_0$.

Based on the above equations, a coupled model (i.e., D-P elastoplastic damage model) is established, and the numerical simulation process is shown in Fig. 8.

Li et al. (2015) pointed that the cumulative acoustic emission energy had an intrinsic consistency with the damage variable E . Taking the mechanical response of KCC as an example, the damage evolution curve of can be easily obtained by acoustic emission experiment data (Fig. 9a). In combination with the parameters from uniaxial and

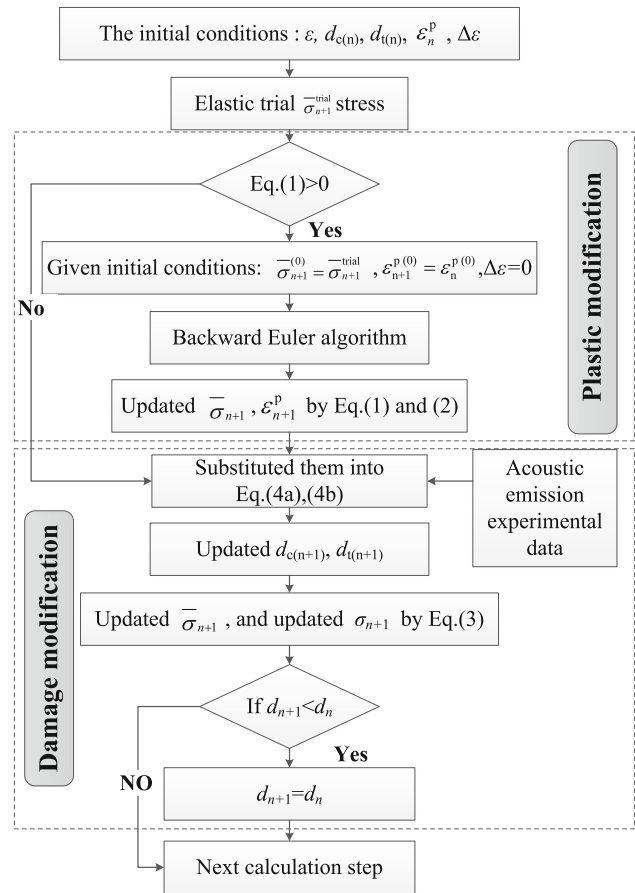


Fig. 8 Numerical calculation process

conventional triaxial test, such as E , ψ , σ_{b0}/σ_{c0} , ε , etc., the stress-strain curve can be calculated by numerical calculation process, as shown in Fig. 8. The calculated results are close to experimental results (Fig. 9b), which shows the rationality of the D-P elastoplastic damage model.

Numerical model and material parameters

According to the geological conditions of Sima mine (Fig. 4), a plane strain numerical model with length of 300 m and height of 150 m was established. This model assumed that the longitudinal profile of the KCC was trapezoid, with a top side 8 m, a bottom side 32 m and a height of 90 m, as shown in Fig. 10. Pressures of 13.93 and 2 MPa were applied on the top and bottom boundary to simulate the vertical stress from the overburden and water pressure in aquifer, respectively. The vertical and horizontal displacement constraints were applied to the model bottom and left and right boundaries, respectively.

In the process of extraction, the goaf area is filled by a soft elastic material to simulate the support capability of the fallen rock from the roof. Based on measured data, 20 m length was added after the first roof caving of 32 m,

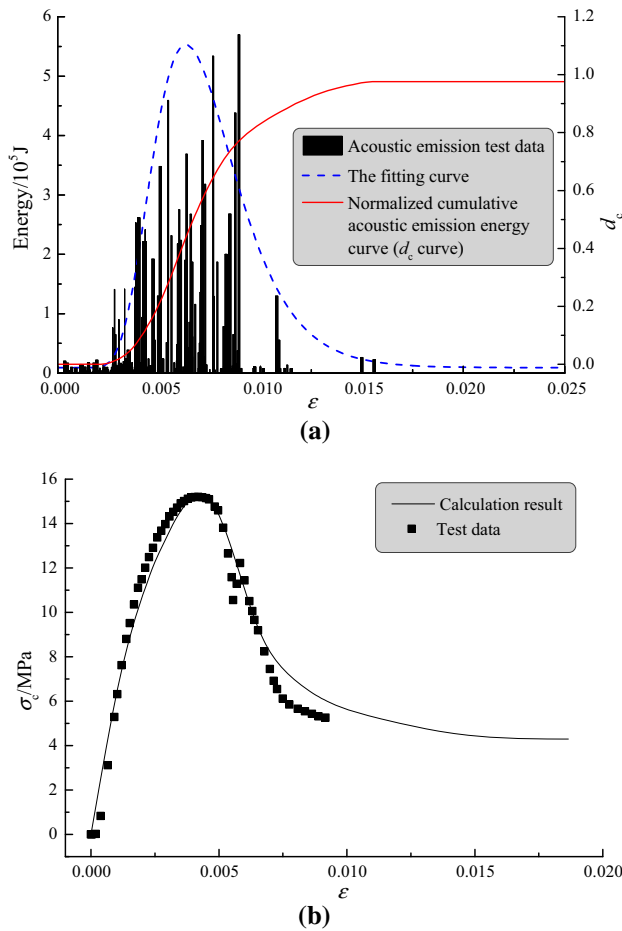


Fig. 9 Verification of D-P elastoplastic damage model. **a** Damage evolution curve (d_c - ϵ) of KCC. **b** Comparison of calculated results and test results

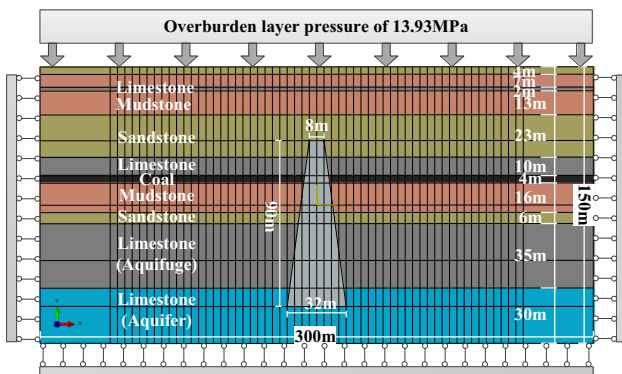


Fig. 10 Numerical calculation model

and backfill of 12 m length was repeatedly added in periodic caving. Young’s modulus for this material is set at 470 MPa, and Poisson’s ratio is 0.25 (Cheng 2010). The mechanical parameters of the remaining materials in the numerical model can be obtained by cyclic loading and unloading experiments and conventional triaxial experiments, as shown in Table 3 and Fig. 11.

Table 3 Mechanical parameters

	ρ (kg/m ³)	E_0 (GPa)	μ	ψ	δ	σ_{b0}/σ_{c0}	K
Coal	2500	3.60	0.3	14	0.1	1.16	0.667
Mudstone	1600	3.53	0.25	15	0.1	1.16	0.667
Sandstone	2500	13.1	0.20	18	0.1	1.16	0.667
Limestone	2600	20.8	0.22	17	0.1	1.16	0.667
KCC	2100	1.87	0.32	11	0.1	1.16	0.667

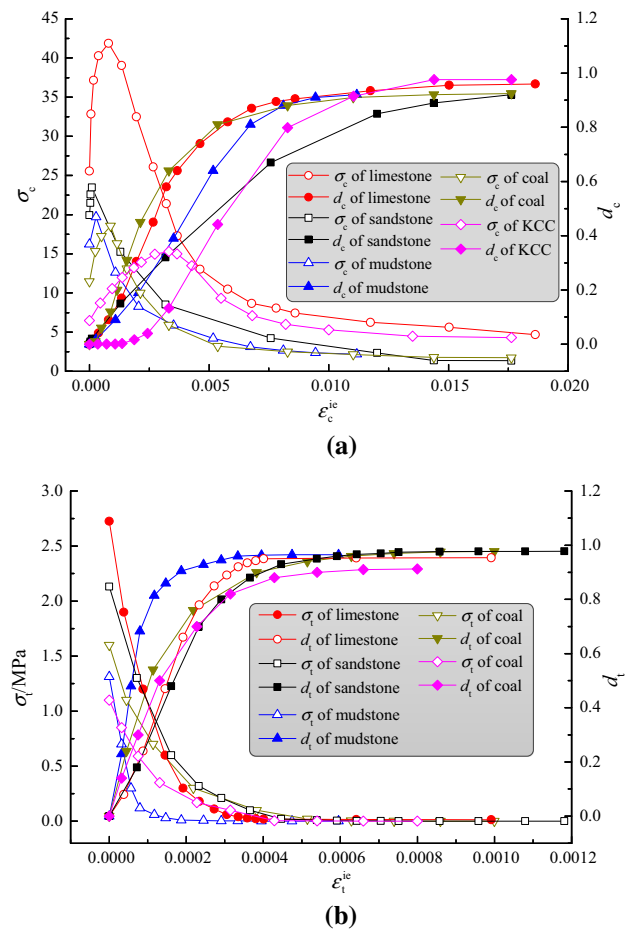


Fig. 11 Damage evolution curves of limestone, sandstone, mudstone, coal and KCC. **a** Relation of d_c - ϵ_c^{ie} and σ_c - ϵ_c^{ie} . **b** Relation of d_t - ϵ_t^{ie} and σ_t - ϵ_t^{ie}

Results and discussion

Using the coordinate system (Fig. 5), Fig. 12 shows the stress and damage results when the distance between mining face and T₂ are -25, -17, -3, 10 and 20 m.

In order to study the damage thickness of floor, shear stress from complete floor and the sidewall of DX1 were analyzed to determine the stress distribution. During the mining process, the KCC underwent the cyclic loading of

compression–tension–compression. Under the coal wall, a bubble-like stress concentration zone was formed. This “bubble” presented a tendency to deform to the goaf ($L_0 = -25, 10, 20$ m) in the complete floor. However, in the KCC, the direction of the “bubble” deformation and mining advance were the same ($L_0 = -17, -3$ m). In the goaf, a shallow, semielliptical stress relief zone was formed. As the roof collapses, the filling body was compacted and the stress in the floor increased again.

Compression damage developed in the above “bubble” area, and its depth determined the floor rupture thickness, which was a key to prevent water inrush from KCC. When the distance between the working face and the KCC exceeds 30 m, the stress within the column changed little, and no damage occurred. With the working face advance, the shear stress had a greater impact on the KCC and suddenly formed a compression damage area of 29.1 m depth at $L_0 = -25$ m. When the coal wall was located at the edge of the KCC, that is, $L_0 = -17$ m or $L_0 = -3$ m, the shear stress in the column reached peak, and the shear stress concentration coefficients are 3.82 and 5.46, respectively, which means that the damage thickness in the right is greater than that in the left. When $L_0 \geq 10$ m, the compressive damage area in the surrounding rock is still increasing. However, the thickness of the compression damage in the KCC is maintained at about 32.5 m, which is less than aquifuge thickness 57 m.

Tensile damage developed in above semielliptical stress relief zone. First compressive damage produced and then tensile damage, resulting in an increase in KCC permeability. In addition, due to the pressure of the No. 7 backfill, the tensile damage thickness in left wall was significantly smaller than that in right wall, at which the groundwater inrush was more likely to occur. The range of tensile damage was increased with the mining advance and remained stable at $L_3 = 30.7$ m. This result was consistent with that of the “second peak of water flow” in the water injection test.

In this article, we investigated the possibility of water inrush from a KCC in Sima mine by using a set of methods, including 3D seismic exploration, connectivity test, water injection test in two sidewalls and numerical simulation based on D–P elastoplastic damage model. The size and type of KCC are determined by the first two, and the damage thickness of KCC is determined by the latter two. Because the KCC belongs to good cementation type (Fig. 4b), the influence of seepage on the KCC is neglected, while the influence of mining and confined water pressure on the KCC is analyzed from the mechanical aspects. Our results showed that the damage distribution in the KCC exhibits an asymmetrical inverted saddle shape, and the maximum damage thicknesses is

located at the sidewall away from the starting cut (Figs. 6, 12). This finding is significant because it clearly indicates the most dangerous position in KCC of good-cementation-type under mining influence. The KCC’s damage thickness was obtained by numerical simulation based on D–P elastoplastic damage model and water injection test in two sidewalls. To our knowledge, these methods were used for the first time in the prevention water inrush from KCC. As is known, the floor is subjected to the cyclic loading of compression–tension–compression during the mining advance (Yin et al. 2016). This loading path makes the rock mechanical properties complicated (Fig. 7). Elasticity theory (Li et al. 2016; Zhang and Tu 2016), elastic–plastic theory (Ou et al. 2013; Yin and Zhang 2005) and elastic damage theory (Zhu and Wei 2011) have been used previously for predicting the safety of the working face. However, the floor damage thickness cannot be concluded from those models because they were conducted by the lack of cycle loading path, lack of plastic strain or lack of elastic modulus reduction. The D–P elastoplastic damage model, which can better represent mining practice, makes the results of numerical simulation more meaningful.

To date, most of researchers used “strain method” in situ test (Zhu and Wei 2011; Yin et al. 2016). This method could partially explain the change in floor stress with the mining advance. But the reason for water inrush from KCC is the development of rock fissures under the mining influence, and there seems to be no direct relationship between fissure and strain (Wang et al. 2012). Although a method of direct testing KCC’s damage was reported in a previous study (Ma et al. 2016) using water injection test, the exact location of the most dangerous position in the KCC was still unclear because they set the test section in the middle of the KCC. In order to obtain damage distribution in the KCC, an improved method named “water injection test in two sidewalls” have been developed. Through the above in situ test and numerical simulation method, we obtained that the KCC is good cementation type. On this basis, we have determined that the most dangerous position in the KCC is at the sidewall away from the starting-cut under the mining influence. This suggests the feasibility of this set of methods in preventing KCC water inrush. The methods would be a valuable tool with applications in karst development areas and cyclic loading and unloading conditions, such as tunneling engineering (Marinos 2001; Filipponi 2015). In addition, it contributes to protect carbonate aquifers, which constitutes a water reserve of critical importance as a source of drinking water (Parise et al. 2008; Jiménez-Madrid et al. 2010).

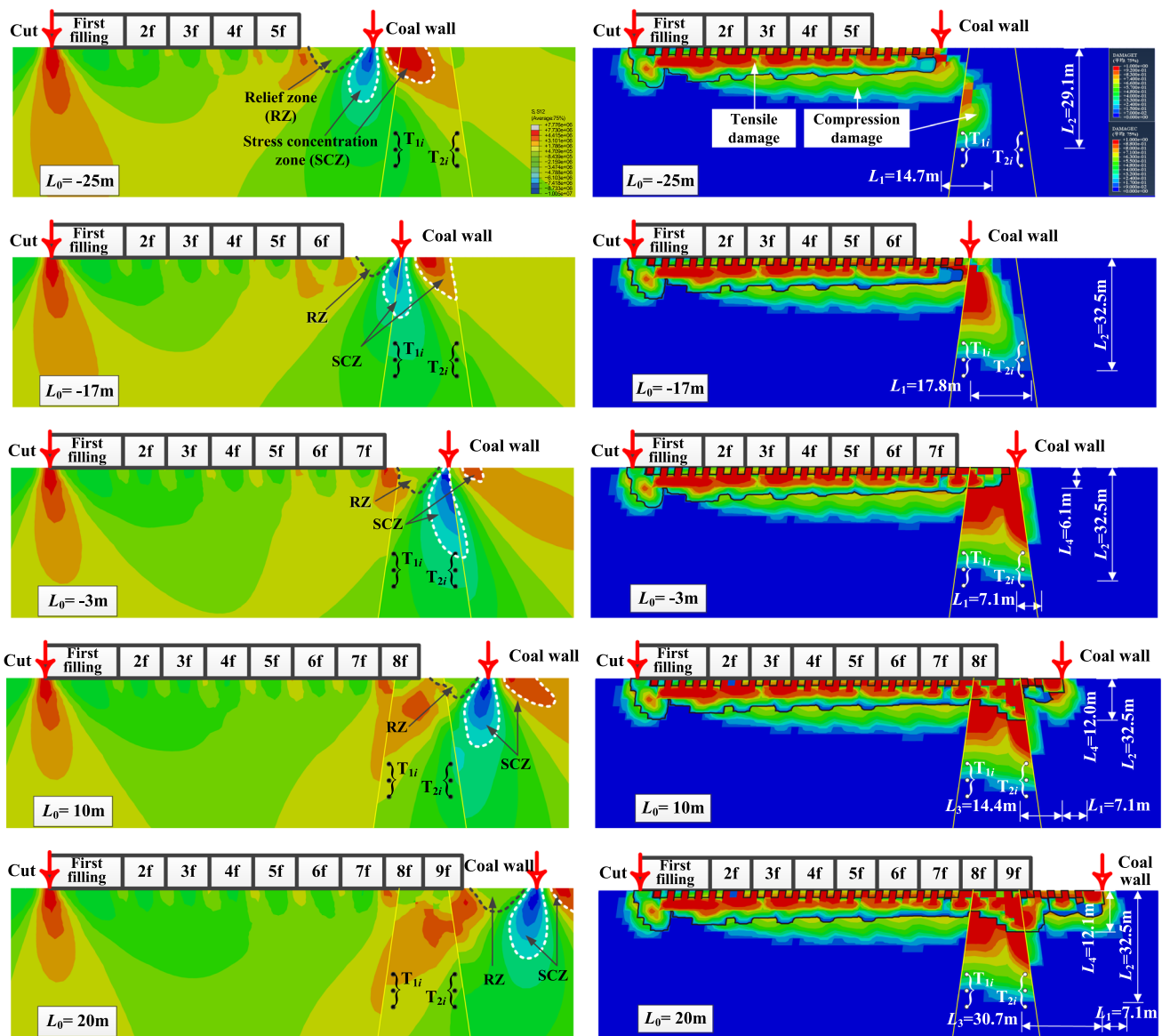


Fig. 12 Results of tensile, compressive damage (*left*) and shear stress (*right*) in floor

Conclusions

The working face has safely passed through the DX1 according to the results of in-site experiments and numerical simulation, and the main conclusions are as follows:

1. By recording the water pressure value of the water injection hole in the connectivity test and whether there is water in the observation hole, it is evaluated that the DX1 is good cementation type and has good water barrier performance under the pressure of 5 Mpa.
2. In the process of mining advance, the shear stress concentration area below the coal wall leads to compressive damage to the rock, and the damage distribution in the KCC exhibits an asymmetrical

inverted saddle shape, and the maximum damage thickness appears when the working surface is at the sidewall during the working face from the KCC to the outside (Figs. 6, 11).

3. The tension damage range increases with the increase in the goaf area and reaches the maximum at the right edge of the KCC (Fig. 11). The tensile damage zone has a strong water conductivity and it is connected with the compressive damage area resulting in the risk of water inrush being further increased at the right sidewall of KCC.

Acknowledgements The author sincerely thanks Mr. Wang Shaojie at Tianjin Chengjian University for providing workstation and related data access. The support of the Research Innovation Program for

College Graduates of Jiangsu Province, under the grants KYLX16_0537, is gratefully acknowledged.

References

- Cheng YM, Wang JA, Xie GX, Wei WB (2010) Three-dimensional analysis of coal barrier pillars in tailgate area adjacent to the fully mechanized top caving mining face. *Int J Rock Mech Min Sci* 47:1372–1383
- Filippini M (2015) Karst risk assessment for underground engineering: Comparison of the KarstALEA method with a random karst distribution approach. In: Lollino G, Manconi A, Guzzetti F, Culshaw M, Bobrowsky P, Luino F (eds) *Engineering Geology Society and Territory*, vol 5. Springer, Cham, pp 603–607
- Hao BY, Zhang YJ, Qi TY, Feng GR, Bai JW, Zhang M, Kang LX (2015) Simulation of interaction between mine-induced stress and stress of collapse column with fully-mechanized working face advancing. *J Min Saf Eng* 32(2):192–198 **(in Chinese and abstract in English)**
- He KQ, Guo D, Du W, Wang R (2007) The effects of karst collapse on the environments in North China. *Environ Geol* 52(3):449–455
- Huang Z, Jiang Z, Qian Z, Cao D (2014) Analytical and experimental study of water seepage propagation behavior in the fault. *Acta Geodyn Geomater* 176:361–370
- Jiménez-Madrid A, Carrasco F, Martínez C (2010) The protection of groundwaters destined for human consumption in karstic aquifers. *Advances towards safeguard zones*. In: Andreo B, Carrasco F, Durán J, LaMoreaux J (eds) *Advances in Research in Karst Media*. Environmental Earth Sciences. Springer, Berlin, Heidelberg, pp 299–304
- Lee J, Fenves GL (1998) Plastic-damage model for cyclic loading of concrete structures. *J Eng Mech* 124:892–900
- Li GY, Zhou WF (2006) Impact of karst water on coal mining in North China. *Environ Geol* 49:449–457
- Li J, Wu JY, Chen JB (2015) *Mechanics of random damage of concrete*. Science Press, Beijing (in Chinese)
- Li Z, Feng G, Zhai C (2016) Study on “triangle” water-inrush mode of strong water-guide collapse column. *J Cent South Univ* 23(9):2402–2409
- Lublimer J, Oliver J, Oller S, Onate E (1989) A plastic-damage model for concrete. *Int J Solids Struct* 25:299–326
- Ma D, Miao X, Bai H (2016) Effect of mining on shear sidewall groundwater inrush hazard caused by seepage instability of the penetrated karst collapse pillar. *Nat Hazards* 82(1):73–93
- Marinos P (2001) Tunnelling and mining in karstic terrane; An engineering challenge. *Geotech Environ Appl Karst Geol Hydrol* 3–16
- Ou S, Wang L, Wang P (2013) Numerical analysis of seepage flow characteristic of collapse column under the influence of mining. *Int J Min Sci Technol* 23(2):237–244
- Parise M, De Waele J, Gutierrez F (2008) *Engineering and environmental problems in karst—an introduction*. Eng Geol 99:91–94
- Qian XP (1988) The formation of gypsum karst collapse-collum and its hydrogeological significance. *Carsol Sin* 4:344–348
- Shi J, Lian D, Yang S (1998) A discussion of karst collapse. *Geol Min Res North China Mag* 13(3):264–266 **(in Chinese and abstract in English)**
- Wang Y, Yang W, Li M, Liu X (2012) Risk assessment of floor water inrush in coal mines based on secondary fuzzy comprehensive evaluation. *Int J Rock Mech Min Sci* 52:50–55
- Wu Q, Fan S, Zhou W, Liu S (2013) Application of the analytic hierarchy process to assessment of water inrush: a case study for the no. 17 coal seam in the Sanhejian Coal Mine, China. *Mine Water Environ* 32:229–238
- Yin SX, Zhang J (2005) Impacts of karst paleo-sinkholes on mining and environment in northern China. *Environ Geol* 48(8):1077–1083
- Yin SX, Wu Q, Wang SX (2005) Water-bearing characteristics and hydro-geological models of karstic collapse columns in north China. *Chin J Rock Mech Eng* 24(1):77–82 **(in Chinese and abstract in English)**
- Yin H, Lefticariu L, Wei J (2016) In situ dynamic monitoring of stress revolution with time and space under coal seam floor during longwall mining. *Environ Earth Sci* 75(18):1249–1260
- Yuan D (1994) *Karstology of China*. Geological Publishing House, Beijing **(in Chinese)**
- Zhang C, Tu S (2016) Control technology of direct passing karstic collapse pillar in longwall top-coal caving mining. *Nat Hazards* 84(1):17–34
- Zhang JF, Zhang HL, Meng D, Cao J (2009) Numerical simulation of rock deformation and seepage field with a fully-water karstic collapse column under mining influence. *Chin J Rock Mech Eng* 28:77–82 **(in Chinese and abstract in English)**
- Zhou ZA, Yang WM (1999) The background of rocks mechanics of karst collapse column in Shanxi. *J China Coal Soc* 24(4):341–344 **(in Chinese and abstract in English)**
- Zhu WC, Wei CH (2011) Numerical simulation on mining-induced water inrushes related to geologic structures using a damage-based hydromechanical model. *Environ Earth Sci* 62(1):43–54